Analyses of temperature-dependent interface states, series resistances, and AC electrical conductivities of Al/p–Si and Al/$Bi_4Ti_3O_{12}$/p–Si structures by using the admittance spectroscopy method

Mert Yıldırım[a)†], Perihan Durmuş[b)], and Şemsettin Altındal[b)]

[a)] *Department of Physics, Faculty of Arts & Sciences, Düzce University, 81620, Düzce, Turkey*
[b)] *Department of Physics, Faculty of Sciences, Gazi University, 06500, Ankara, Turkey*

(Received 26 December 2012; revised manuscript received 10 April 2013)

In this study, Al/p–Si and Al/$Bi_4Ti_3O_{12}$/p–Si structures are fabricated and their interface states (N_{ss}), the values of series resistance (R_s), and AC electrical conductivity (σ_{ac}) are obtained each as a function of temperature using admittance spectroscopy method which includes capacitance–voltage (C–V) and conductance–voltage (G–V) measurements. In addition, the effect of interfacial $Bi_4Ti_3O_{12}$ (BTO) layer on the performance of the structure is investigated. The voltage-dependent profiles of N_{ss} and R_s are obtained from the high–low frequency capacitance method and the Nicollian method, respectively. Experimental results show that N_{ss} and R_s, as strong functions of temperature and applied bias voltage, each exhibit a peak, whose position shifts towards the reverse bias region, in the depletion region. Such a peak behavior is attributed to the particular distribution of N_{ss} and the reordering and restructuring of N_{ss} under the effect of temperature. The values of activation energy (E_a), obtained from the slope of the Arrhenius plot, of both structures are obtained to be bias voltage-independent, and the E_a of the metal–ferroelectric–semiconductor (MFS) structure is found to be half that of the metal–semiconductor (MS) structure. Furthermore, other main electrical parameters, such as carrier concentration of acceptor atoms (N_A), built-in potential (V_{bi}), Fermi energy (E_F), image force barrier lowering ($\Delta\Phi_b$), and barrier height (Φ_b), are extracted using reverse bias C^{-2}–V characteristics as a function of temperature.

Keywords: MFS structures, Bismuth titanate, temperature dependent, activation energy, AC electrical conductivity

PACS: 85.30.Hi, 85.30.Kk, 84.37.+q **DOI:** 10.1088/1674-1056/22/10/108502

1. Introduction

In recent years, materials with high dielectric constants, such as Si_3N_4, TiO_2, and $Bi_4Ti_3O_{12}$ (BTO), have been chosen instead of materials with low dielectric constants, such as conventional SiO_2 and SnO_2. This is because high dielectric materials lead to a considerable reduction in both the leakage current and the series resistance of devices. As a member of the high-κ material family, BTO has a high dielectric constant and therefore it improves the leakage current through providing a higher shunt resistance (R_{sh}). On the other hand, owing to its low coercive field which is suitable for nonvolatile memory applications, high Curie temperature which minimizes thermal depolarization problems, high dielectric constant, high breakdown strength, and peculiar switching behavior, BTO has attracted considerable attention in the applications of memory storage capacitors, optical memories, and electro–optic devices.[1–10] Moreover, due to its unique properties mentioned above, BTO is used as a ferroelectric thin film in memory applications such as ferroelectric random access memory (FeRAM) where a metal–ferroelectric–metal (MFM) capacitor is used,[8] and ferroelectric field effect transistors (FeFETs) where ferroelectric material is used as the gate oxide in the form of metal–ferroelectric–semiconductor (MFS) or metal–ferroelectric–insulator–semiconductor (MFIS) structures.[11–14] In an MFS structure, the surface potential of the semiconductor is controlled by the remnant polarization of the ferroelectric thin film,[15] therefore ferroelectric materials are chosen in memory applications such as FeRAMs, FeFETs, etc.

MFS structures were first proposed by Wu[16] and preceding his proposal, researchers conducted various studies on these structures and possible suitable ferroelectric materials.[17–22] What makes MFS structures a good alternative to MIS structures is the high dielectric constant and large polarization field of the ferroelectric material. Also, better admittance characteristics (capacitance–voltage (C–V) and conductance–voltage (G–V)) can be obtained even under low bias voltages, owing to the ferroelectric interfacial layer. In addition to this, series resistance (R_s) is also an important parameter which affects the electrical characteristics of the device in many ways because the applied bias voltage across the structure will be shared by the ferroelectric layer, depletion region, and R_s of the device. High-κ materials cause improvements by ensuring lower R_s and N_{ss}, therefore they have a positive effect on structural performance and efficiency. Furthermore, inserting high-κ thin film between the metal and the semiconductor prevents interaction and interdiffusion between them, thereby leading to further improvements.

Admittance spectroscopy (AS) considers the contribution from majority-carrier trapping defects through capaci-

†Corresponding author. E-mail: mertyildirim@duzce.edu.tr

© 2013 Chinese Physical Society and IOP Publishing Ltd

tance measurements using small ac signal. In this respect, AS has been proven to be a powerful technique in order to obtain bulk or interface defect properties. Over the past few decades, AS has been considered as a great tool to extract structural parameters such as density of interface traps, activation energy, etc. of structures such as metal–semiconductors (MSs), MIS, and MFS.[23–25] Although, there are studies in which MFS structures were characterized by various methods, we believe that further studies under various conditions are necessary to understand electrical characteristics of MFS structures explicitly. The purpose of this study is to reveal the effects of a BTO layer and temperature on the main electrical parameters of Al/p–Si structures, therefore in this study we investigate the changes occurring after ferroelectric BTO layer deposition using the admittance measurements of Al/p–Si (MS) and Al/BTO/p-Si (MFS) structures in a temperature range between 120 K–300 K.

2. Experimental details

P-type Si substrate was degreased in organic solvents of $CHClCCl_2$, CH_3COCH, and CH_3OH consecutively, and then etched sequentially in H_2SO_4 and H_2O_2, 20% HF, a solution of $6HNO_3$:1 HF:35 H_2O, 20% HF and finally quenched in de-ionized water for a prolonged time. Preceding each cleaning step, the substrate was rinsed thoroughly in de-ionized water of resistivity of 18 MΩ·cm. Then, in order to fabricate the MFS structure, the ferroelectric $Bi_4Ti_3O_{12}$ (BTO) thin film was deposited on Si substrate with RF magnetron sputtering by using a hot compaction of $Bi_4Ti_3O_{12}$ powder of a stoichiometric composition as a target material. This step was skipped for the fabrication of the MS structure. The mixture of argon (Ar) and oxygen (O_2) was used as a working medium and the substrate was kept at 700 °C. The thickness of $Bi_4Ti_3O_{12}$ was obtained to be about 90 Å. The Ohmic contacts were prepared by sintering the evaporated back contact at about 600 °C for 20 minutes under a dry nitrogen (N_2) ambient at a rate of 1.5 l/min. This process was for sintering the Au on upper surface of the p-type Si substrate. For electrical measurements, pure Al (99.999%) circular dots with an average thickness of about ∼ 2000 Å and a diameter of 1 mm were deposited by a metal evaporation system through a shadow mask on the BTO film. In this way, an MFS structure was fabricated on the p-Si substrate. The structure was mounted on a copper holder with the help of silver paste and the electrical contacts of the upper electrodes were made by using tiny silver coated wires with silver paste. *C*–*V* and *G*–*V* measurements of MS and MFS structures were carried out in Janis vpf-475 cryostat in a temperature range of 120 K–300 K. Admittance measurements of the structures were conducted using an HP4192A LF impedance analyzer with a small ac test signal of 40 mV_{rms} using a microcomputer through an IEEE-488 AC/DC converter card.

3. Results and discussion

C–*V* and G/ω–*V* plots of MFS structure at various temperatures are given in Figs. 1 and 2, respectively, with their insets reflecting the same plots of MS structure. As can be seen in these figures, *C* and *G* show a strong dependence on temperature and applied bias voltage. *C*–*V* and G/ω–V plots of MFS structure exhibit inverse, depletion, and accumulation regions, and the observed behaviors of these plots resemble those of MIS structures. The changes in *C* and *G* become more distinctive especially in the depletion region rather than other regions due to the effect of N_{ss}, which are localized between semiconductor and ferroelectric layer. It is clear that in the accumulation region the *C*–*V* and G/ω–*V* plots of the MFS structure show more obvious peaks than those of the MS structure. The origins of such peak behavior in *C*–*V* and G/ω–*V* plots can be attributed to, especially, R_s rather than N_{ss}.[25–28] On the other hand, contrary to *C*–*V* plots of the MFS structure, those of the MS structure display peak behaviors in the depletion region, owing to the effect of N_{ss}. This indicates that BTO layer causes the passivation of N_{ss} in this region. These results show that N_{ss} is more effective in the depletion region while R_s is more effective in the accumulation region. As seen in Fig. 1, *C*–*V* plots of both structures bend even more as the temperature increases, which suggests that R_s takes larger values at high temperatures, which is in contrast to what is expected. Also, the dispersion in *C* values becomes narrower in the high forward bias region, which implies that the temperature dependence of *C*–*V* plot of the MFS structure weakens as the applied bias voltage increases. As to the effects of the BTO layer on *C* and *G*, one can see that *C* and G increase after the deposition of BTO layer as a result of the high dielectric constant of BTO. Moreover, as expected, better switching behavior occurs due to BTO's peculiar switching ability. However, as shown in the figures, the switching performance of BTO scales down at low temperatures.

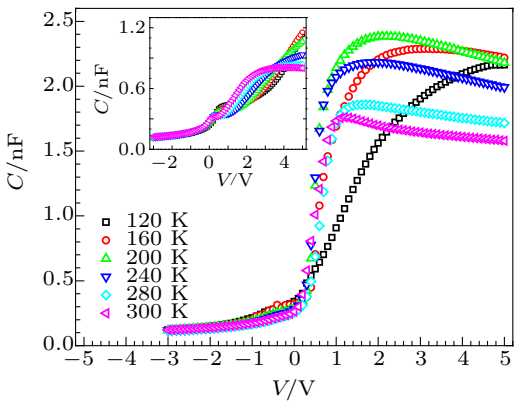


Fig. 1. (color online) *C*–*V* plots of the MFS structure at various temperatures, with the inset showing the *C*–*V* plots of the MS structure.

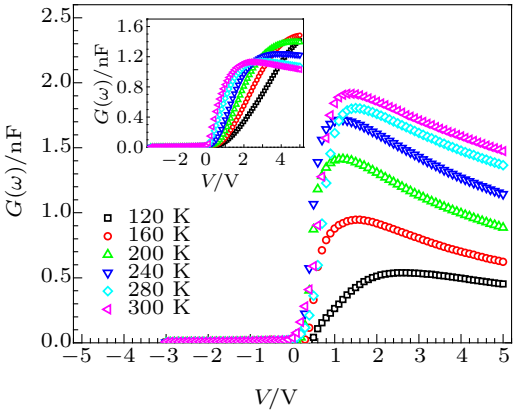


Fig. 2. (color online) G/ω–V plots of the MFS structure at various temperatures, with the inset showing the G/ω–V plots of the MS structure.

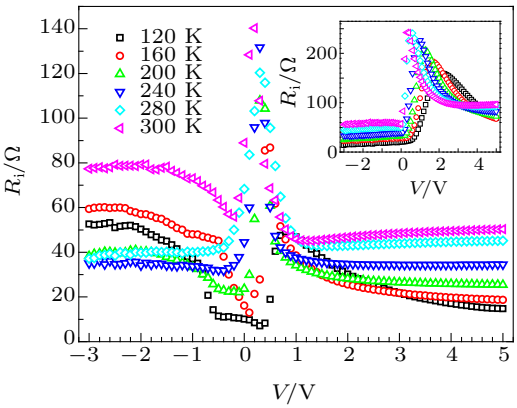


Fig. 3. (color online) R_i–V plots of the MFS structure at various temperatures, with the inset showing the R_i–V plots of the MS structure.

As mentioned earlier, the R_s of a structure affects it in various ways; some of which can be listed as peak behaviors in C–V and G/ω–V plots, lower bias voltage felt by the structure as a result of voltage drop caused by R_s, etc.[25–30] The most commonly used practical method for obtaining the real value of R_s of a structure was introduced by Nicollian and Brews,[23] and it is expressed as

$$R_s = \frac{G_{ma}}{G_{ma}^2 + (\omega C_{ma})^2}. \quad (1)$$

Here C_{ma} and G_{ma} are the measured C and G values in the strong accumulation region, respectively. Equation (1) can also be used for obtaining the value of voltage-dependent resistance (R_i) at any bias voltage in general. R_i–V plots of the MFS structure are given in Fig. 3, with the inset showing those of the MS structure. As shown in Fig. 3, the value of R_i increases in general as the temperature increases. The values of these plots in the strong accumulation region correspond to R_s values. Comparing Fig. 3 and its inset, it is seen that R_s takes lower values after deposition of BTO. For a better comparison, R_s–T plots of MS and MFS structures are given in Fig. 4. As shown in Fig. 4, thanks to the BTO layer, lower R_s values are obtained. On the other hand, R_s increases with temperature increasing. This behavior is in contrast to the expected negative temperature coefficient of R_s. However, considering the distinctive peak behaviors in C–V and $G(\omega)$–V observed at high temperatures, it is not surprising to have higher R_s at high temperatures. Also, such a behavior can be attributed to the lack of free space charges at low temperatures.

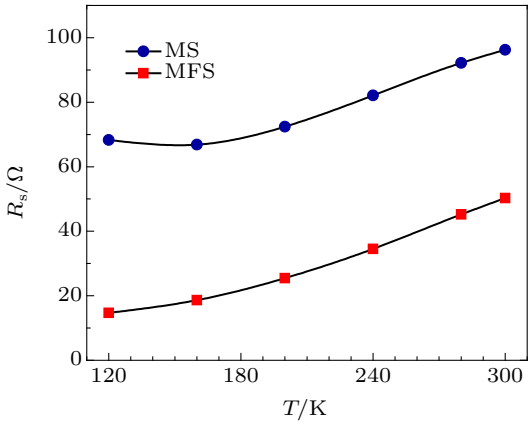


Fig. 4. (color online) R_s–T plots of MS and MFS structures.

Besides R_s, N_{ss} is also an important parameter affecting a structure's electrical characteristics. Reported studies made it clear that deviation of a structure's electrical characteristics from the ideality becomes explicit if admittance measurements are conducted at low frequencies. Also, conducting the measurements at low frequencies leads to higher N_{ss} values depending on the relationship between carrier lifetime of charges and ω^{-1}.[23,31–33] The effect of N_{ss} is tried to be kept as minimal as possible by conducting the measurements at 1 MHz since the trapped charges at interface states cannot follow ac signal at sufficiently high frequencies. Nevertheless, the trapped charges may have different lifetimes depending on temperature, and hence some of them may still follow the ac signal and contribute to total capacitance. Therefore, it is of interest to investigate N_{ss} as well. Among the various methods of obtaining N_{ss}, the conductance method developed by Nicollian and Goetzberger[33] is generally thought to be the most accurate. However, this method is very time consuming since it requires separate measurements of C and G at high frequencies. On the other hand, the high–low frequency capacitance method is a practical method which requires less time for obtaining the bias voltage distribution profile of N_{ss}. Moreover, this method yields values that are quite close to those obtained when using the conductance method. This method derives N_{ss} from the excess capacitance, which emerges due to the charges that are able to follow ac signal, using the following relationship:

$$N_{ss} = \frac{1}{qA}\left[\left(\frac{1}{C_{LF}} - \frac{1}{C_{ox}}\right)^{-1} - \left(\frac{1}{C_{HF}} - \frac{1}{C_{ox}}\right)^{-1}\right], \quad (2)$$

where C_{LF}, C_{HF}, and C_{ox} are low-frequency, high-frequency, and oxide capacitance, respectively, q is electronic charge and A is the rectifying contact area. The values of N_{ss} of both structures are obtained using Eq. (2), and N_{ss}–V plots of MFS and

MS structures are given in Fig. 5 and its inset, respectively. It is seen that N_{ss} of the MFS structure takes smaller values than those of the MS structure, owing to passivation through the BTO layer. Also, N_{ss} of the MFS structure increases as the temperature increases; such a behavior of N_{ss} can be attributed to molecular restructuring and reordering of surface charges under the effect of temperature. Moreover, it is seen that the obtained N_{ss} values for the MFS structure are of the same order as those obtained by Parlaktürk *et al.*[17] and Bülbül *et al.*[34]

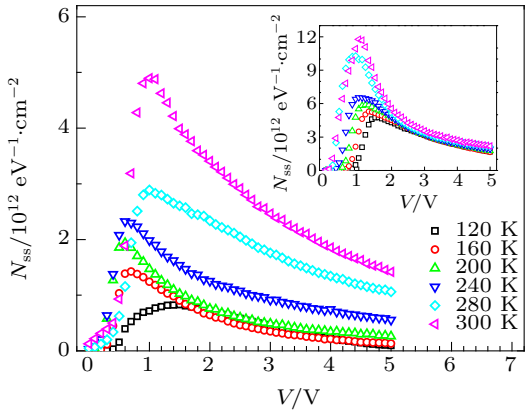


Fig. 5. (color online) N_{ss}–V plots of the MFS structure at various temperatures, with the inset showing the N_{ss}–V plots of the MS structure.

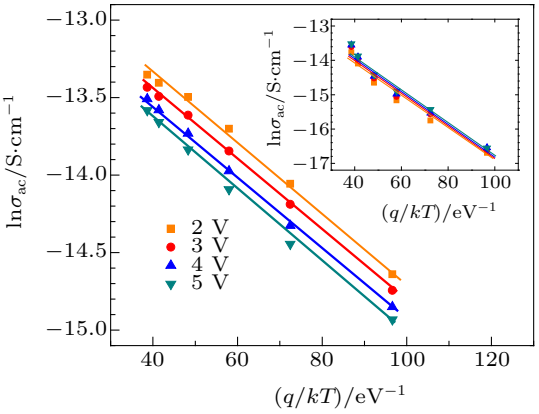


Fig. 6. (color online) ln σ_{ac}–q/kT plots of the MFS structure, with the inset showing the ln σ_{ac}–q/kT plots of the MS structure.

Activation energy (E_a) is another structural parameter investigated in the scope of this study. E_a values are extracted using AC conductivity (σ_{ac}) which is given by the following equations: [25]

$$\sigma_{ac} = \frac{G\delta}{A}, \tag{3a}$$

$$\sigma_{ac}(T) = \sigma_o \, e^{-qE_a/kT}, \tag{3b}$$

where δ is the thickness of the insulating layer, which is the BTO layer in our case, σ_o is the pre-exponential factor, k is the Boltzmann constant, and T is absolute temperature in Kelvin. Firstly, σ_{ac} values are calculated through Eq. (3a) and then the obtained values are utilized in Eq. (3b) such that slope of ln σ_{ac}–q/kT plot yields the value of E_a. Therefore, ln σ_{ac}–q/kT plots of MFS structure at various bias voltages are obtained and given in Fig. 6 where the inset shows ln σ_{ac}–q/kT plots of MS structure. As shown in Fig. 6, ln σ_{ac}–q/kT plots present linear behaviors in the whole temperature range and slopes of these plots are almost constant with applied bias voltage. E_a values at 2, 3, 4, and 5 V are extracted to be 22.4, 22.9, 23.3, and 23.5 meV for MFS structure and 48.7, 49.0, 49.4, and 49.6 meV for MS structure respectively. It is obvious that deposition of the BTO layer reduces the E_a value almost by half. Also, it is seen that E_a values are independent of bias voltage.

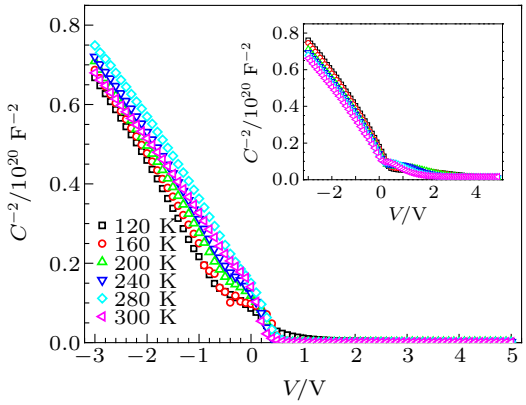


Fig. 7. (color online) C^{-2}–V plots of MFS structures, with the inset showing the C^{-2}–V plots of the MS structure.

Besides σ_{ac}, some main electrical parameters of MS and MFS structures are obtained using the depletion layer capacitance approach on C^{-2}–V plots given in Fig. 7. The relationship between C and V in the depletion region is given by[23,29,35]

$$C^{-2} = \frac{2}{q\varepsilon_s A^2 N_A}\left(V_{bi} + V\right). \tag{4}$$

Here, ε_s, N_A, and V_{bi} are permittivity of the semiconductor, carrier concentration of the acceptor atoms or acceptor doping concentration, and built-in potential, respectively. N_A and V_{bi} are extracted from the slope and intersection point of the linear sections of C^{-2}–V plots. After N_A values are extracted, Fermi energy (E_F) values are calculated by using the following equation:[23,29]

$$E_F = \frac{kT}{q}\ln\left(\frac{N_V}{N_A}\right). \tag{5}$$

Here, N_V is the effective density of states in the valance band. Finally, barrier height (Φ_b) values are obtained using E_F and V_{bi} in the following equation:[23,25,29,35]

$$\Phi_b = qV_{bi} + \frac{kT}{q} + E_F - \Delta\Phi_b, \tag{6}$$

where $\Delta\Phi_b$ is the image force barrier decrement whose acquisition is given in Refs. [23] and [25]. The obtained values of these electrical parameters are given in Table 1. As can be seen, the increasing temperature caused all parameters, except E_F, of both structures to have smaller values. As to the changes observed after deposition of the BTO layer, Fig. 8 shows the

effect of the BTO layer on Φ_b. As can be seen in Fig. 8, the BTO layer causes MS and MFS structures to have lower values in the low temperature region whereas the opposite behavior is obtained for the high temperature region. Regarding the temperature dependence of Φ_b, the following equation holds:[36]

$$\Phi_b(T) = \Phi_b(0\ \mathrm{K}) + \alpha T, \tag{7}$$

where Φ_b (0 K) is the barrier height at absolute zero Kelvin and α is the negative temperature coefficient of barrier height. As shown in Fig. 8, Φ_b (0 K) and α of the MFS structure take values of 0.807 eV and -5.4×10^{-4} eV/K whereas those of the MS structure are 1.027 eV and -16×10^{-4} eV/K. The BTO layer causes the MFS structure to have an α value that is quite close to the negative temperature coefficient of the band gap for silicon (-4.73×10^{-4} eV/K). This result shows that the temperature-dependent barrier height values obtained from the reverse bias of C–V are quite reliable.

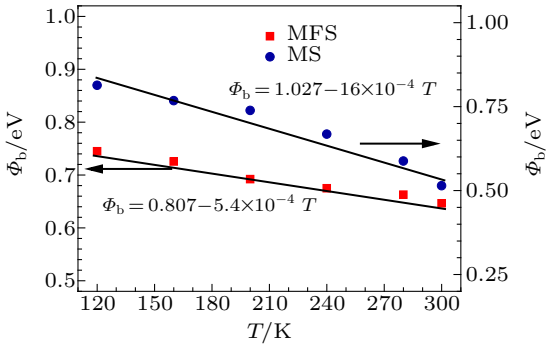


Fig. 8. (color online) Φ_B–T plots of MS and MFS structures.

Table 1. Electrical parameters of MS and MFS structures at various temperatures.

T/K	MS					MFS				
	$N_A/10^{-14}$ cm^{-3}	qV_{bi}/eV	E_F/eV	$\Delta\Phi_b$/meV	Φ_b/eV	$N_A/10^{-14}$ cm^{-3}	qV_{bi}/eV	E_F/eV	$\Delta\Phi_b$/meV	Φ_b/eV
120	1.76	0.699	0.113	8.7	0.814	3.43	0.638	0.106	10.0	0.745
160	1.60	0.610	0.152	8.2	0.768	1.77	0.569	0.151	8.3	0.725
200	1.64	0.540	0.190	7.9	0.739	1.75	0.494	0.188	8.0	0.692
240	1.48	0.425	0.230	7.4	0.668	1.52	0.433	0.229	7.5	0.675
280	1.75	0.307	0.264	7.0	0.588	1.39	0.376	0.269	7.1	0.663
300	1.48	0.208	0.287	6.3	0.514	1.17	0.334	0.293	6.6	0.646

4. Conclusions

Electrical characteristics of MS and MFS structures are investigated using C–V and G–V measurements at various temperatures. The obtained voltage-dependent profiles of N_{ss} and R_s from the high–low frequency capacitance method and the Nicollian method show that both N_{ss} and R_s are strong functions of temperature and applied bias voltage, and they each give a peak in the depletion region and the peak position shifts towards the reverse bias region. Such a peak behavior is attributed to particular distributions of N_{ss} and their reordering and restructuring under temperature effect. In addition, the value of E_a of the MFS structure is obtained from the slope of the Arrhenius plot to be about 20 meV, which is half that of the MS structure. Barrier height values for MS and MFS structures obtained from reverse bias C–V data decrease with temperature increasing, and temperature coefficient values are found to be -16×10^{-4} eV/K and -5.4×10^{-4} eV/K, respectively. Also, the negative temperature coefficient of the barrier height value of the MFS structure is in good agreement with the negative temperature coefficient of the band gap for silicon (-4.73×10^{-4} eV/K). A comparison between the results for MS and MFS structures suggests that BTO is an outstanding interfacial layer material since better performance and reliability can be obtained in the studied temperature range.

References

[1] Yang H, Ren Q, Zhang G, Chow Y T, Chan H P and Chu P L 2005 *Opt. Laser Technol.* **37** 259

[2] Lin X, Guan Q F, Liu Y and Li H B 2010 *Chin. Phys. B* **19** 107701

[3] Wu Y Y, Wang X H and Li L T 2010 *Chin. Phys. B* **19** 037701

[4] Jo W, Cho H J, Noh T W, Cho Y S, Kwun S I, Byun Y T and Kim S H 1994 *Ferroelectrics* **152** 139

[5] Scott J F 1998 *Ferroelectrics Rev.* **1** 1

[6] Joshi P C, Krupanidhi S B and Mansingh A 1992 *J. Appl. Phys.* **72** 5517

[7] Fouscova A and Cross L E 1968 *J. Appl. Phys.* **39** 2268

[8] Simoes A Z, Gonzalez A H M, Riccardi C S, Souza E C, Moura F, Zaghete M A, Longo E and Varela J A 2004 *J. Electroceram.* **13** 65

[9] Cui C E, Huang P and Xu T X 2006 *Acta Phys. Sin.* **55** 1464 (in Chinese)

[10] Lue Y G, Liang X L, Tan Y H, Zheng X J, Gong Y Q and He L 2011 *Acta Phys. Sin.* **60** 027701 (in Chinese)

[11] Shao T Q, Ren T L, Wei C G, Wang X N, Li C X, Liu J S, Liu L T, Zhu J and Li Z J 2003 *Integr. Ferroelectr.* **57** 1241

[12] Ishiwara H 2004 *Top. Appl. Phys.* **93** 233

[13] Xu Z, Goux L, Kaczer B, Vander Meeren H, Wouters D J and Grouseneken G 2006 *Microelectron. Eng.* **83** 2564

[14] Bozgeyik M S, Cross J S, Ishiwara H and Shinozaki K 2010 *Microelectron. Eng.* **87** 2173

[15] M Okuyama and Y Ishibashi 2005 *Ferroelectric Thin Films Basic Properties and Device Physics for Memory Applications* (New York: Springer)

[16] Wu S Y 1974 *IEEE Trans. Electron. Dev.* **ED-21** 499

[17] Parlaktürk F, Altındal Ş, Tataroğlu A, Parlak M and Agasiev A A 2008 *Microelectron. Eng.* **85** 81

[18] Yoon S M, Tokumitsu E and Ishiwara H 2000 *IEEE Trans. Electron. Dev.* **47** 1630
[19] Gökçen M and Yıldırım M 2012 *Chin. Phys. B* **21** 128502
[20] Tataroğlu A, Altındal Ş, Aydemir U and Uslu H 2010 *Optoelectron. Adv. Mat.* **4** 616
[21] Lin X, Guan Q F, Liu Y and Li H B 2010 *Chin. Phys. B* **19** 107701
[22] Wu Y Y, Wang X H and Li L T 2010 *Chin. Phys. B* **19** 037701
[23] Nicollian E H and Brews J R 1982 *MOS (Metal Oxide Semiconductor) Physics and Technology* (New York: Wiley)
[24] Walter T, Herberholz R, Muller C and Schock H W 1996 *J. Appl. Phys.* **80** 4411
[25] Yıldırım M, Eroğlu A, Altındal Ş and Durmuş P 2011 *J. Optoelectron. Adv. M.* **13** 98
[26] Chattopadhyay P and Raychaudhuri B 1993 *Solid State Electron.* **36** 605
[27] Gökçen M, Altuntaş H and Altındal Ş 2008 *Optoelectron. Adv. Mat.* **2** 838
[28] Dökme İ and Altındal Ş 2011 *IEEE Trans. Electron Dev.* **58** 4042
[29] Dökme İ, Durmuş P and Altındal Ş 2008 *Nucl. Instrum. Method B* **266** 791
[30] Altındal Ş and Uslu H 2011 *J. Appl. Phys.* **109** 074503
[31] Uslu H, Dökme İ, Afadiyeva I M and Altındal Ş 2010 *Surf. Interface Anal.* **42** 807
[32] Xiao H and Huang S 2010 *Mater. Sci. Semicond. Proc.* **13** 395
[33] Nicollian E H and Goetzberger A 1967 *Bell. System Tech. J.* **46** 1055
[34] Bülbül M M, Altındal Ş, Parlaktürk F and Tataroğlu A 2011 *Surf. Interface Anal.* **43** 1561
[35] Pakma O, Serin N, Serin T and Altındal Ş 2009 *J. Sol-Gel Sci. Technol.* **50** 28
[36] Bengi A, Altındal Ş, Özçelik S, Agaliyeva S T and Mammadov T S 2008 *Vacuum* **83** 276